IAHR AIRH

Journal of Hydraulic Research Vol. 46, No. 1 (2008), pp. 4–14

Flow patterns in nappe flow regime down low gradient stepped chutes

Configurations des écoulements en nappe le long des déversoirs en gradins à pente faible

L. TOOMBES, *Connell Wagner, 433 Boundary St, Spring Hill 4000, Australia; Formerly Department of Civil Engineering, The University of Queensland, Brisbane QLD 4072, Australia*

H. CHANSON, IAHR Member, Professor in Civil Engineering, *The University of Queensland, Brisbane QLD 4072, Australia. Fax: (61 7) 33 65 45 99; e-mail: h.chanson@uq.edu.au; http://www.uq.edu.au/~e2hchans/ (author for correspondence)*

ABSTRACT
Although modern gravity dam spillways include often steep chutes operating in skimming flow regime, succession of free-falling nappes (i.e. nappe flow regime) are more common on low gradient chutes and cascades, and this flow situation received little attention to date. New experiments were conducted in nappe flows without hydraulic jump in two large-size facilities with flat slopes. The flow on the stepped cascade displayed complex, three-dimensional patterns. Detailed air–water flow measurements were performed in the jet, at nappe impact and in the downstream flow region. Key results demonstrated that the flow on each step was rapidly varied, highly three-dimensional and strongly aerated.

RÉSUMÉ
Bien que les déversoirs modernes de barrage poids incluent souvent des pentes raides fonctionnant en régime écumant, les successions de nappes en chute libre (i.e. régime d'écoulement en nappe) sont plus courantes sur les déversoirs et les cascades à pentes faibles, or cette forme d'écoulement n'a reçu que peu d'attention jusqu'ici. De nouvelles expériences ont été entreprises sur des écoulements en nappe sans ressaut hydraulique dans deux équipements de grande taille avec des pentes faibles. L'écoulement, sur une cascade en gradin présentait des configurations tridimensionnelles complexes. Des mesures détaillées de l'écoulement air-eau ont été effectuées dans le jet, à l'impact de la nappe et dans la zone d'écoulement aval. Les résultats principaux ont démontré que l'écoulement sur chaque marche était rapidement variable, largement tridimensionnel et fortement aéré.

Keywords: Spillways, stepped channels, low gradient, nappe flow regime, air–water flow, three-dimensional flow patterns, cascades.

1 Introduction

During the 19th century, overflow stepped spillways were selected frequently with nearly one-third of dams built in Europe and North America equipped with a stepped cascade. More recently, the 1980s and 1990s were marked by a regain of interest for that type of spillway design (e.g. Chanson, 2001). Most structures were steep chutes for gravity dams operating in skimming flow regime. For relatively low flow rates, however, the waters cascade down a stepped chute as a succession of free-falling nappes: i.e. nappe flow regime. This flow situation received little attention with some exceptions (e.g. Horner, 1969; Chamani and Rajaratnam, 1994; Chanson, 1994; Pinheiro and Fael, 2000).

It is the purpose of this paper to detail the complicated flow patterns in nappe flow regime down low gradient chutes. The study is supported by new experimental works in large-size facilities under controlled flow conditions, including new air–water flow measurements. The results provide a detailed characterization of the three-dimensional nature of nappe flow regime on flat slope stepped chutes.

2 Experimental apparatus and instrumentation

Experiments were performed in two channels (Table 1). A 25 m long 0.5 m wide flume was designed with a stepped invert consisting of ten 0.143 m high horizontal steps. A second channel (3.2 m long) was equipped with a single step to investigate the flow patterns and air entrainment at and downstream of the first drop. Both channels were flat waterways (bed slope $S_o = 0.065$ and 0.045) with supercritical inflow conditions: $2 \leq Fr_o \leq 10$ where Fr_o is the approach flow Froude number.

The flow rates were measured with a Dall tube flowmeter, calibrated on site, for the 25 m long chute, and a V-notch weir in the 3.2 m long channel. The accuracy on the discharge measurement was about 2%. Clear-water flow depths and velocities were measured with a point gauge and a Prandtl–Pitot tube (Ø = 3.3 mm), respectively. Nappe subpressures were measured with a Projection Manometer. The pressure tapping was located on the centreline, 110 mm above the invert of the lower step and 17 mm from the vertical step face.

Air–water flow properties were measured using either a single-tip conductivity probe (Ø = 0.35 mm) or a double-tip

Revision received November 17, 2005/Open for discussion until August 31, 2008.

Table 1 Experimental flow conditions (present study)

Ref. (1)	Slope θ (deg.) (2)	h (3)	l (4)	q_w m^2/s (5)	d_c/h	Re	Comments (8)
Series 1	3.4	0.143	2.4	0.038–0.163	0.36–0.97	1.5–6.5E + 5	$L = 25$ m, $W = 0.5$ m. Horizontal timber steps. (No sidewall offset at 1st drop.) Nozzle depth: 0.03 m.
Series 2	3.4	0.143	2.4	0.080–0.150	0.6–0.92	3.2–6E + 5	$L = 25$ m, $W = 0.5$ m. Horizontal timber steps. Sidewall offset for nappe ventilation at 1st drop. Nozzle depth: 0.03 m.
Series 3	2.6	0.143	N/A	0.07–0.140	0.5–0.88	2.8–5.6E + 5	Single horizontal perspex step and glass flume. $L = 3.2$ m, $W = 0.25$ m. Sidewall offset for nappe ventilation at drop. Nozzle depth: 0.024–0.04 m.

Notes: θ: pseudo-bed slope formed by step edges; d_c: critical flow depth; h: step height; Re: Reynolds number defined in terms of hydraulic diameter; W: channel width.

conductivity probe ($\O = 0.025$ mm) developed at the University of Queensland. The probes were aligned in the flow direction and excited by an air bubble detector (AS25240). The resistivity probe signals were scanned at 5 and 40 kHz, respectively, for the single-tip and double-tip resistivity probes. The translation of the probes in the direction normal to the channel invert was controlled by a fine adjustment travelling mechanism connected to a MitutoyoTM digimatic scale unit (Ref. No. 572-503). The error on the vertical position of the probe was less than $\Delta z < 0.025$ mm. The system (probe and travelling mechanism) was mounted on a trolley system. The accuracy on the longitudinal position of the probe was estimated as $\Delta x < 0.5$ cm. The accuracy on the transverse position of the probe was estimated as $\Delta y < 0.5$ mm.

Further information and details were provided in Toombes (2002).

2.1 Inflow conditions

The flow to the 25 m long flume was fed through a smooth convergent nozzle (1.7 m long), the nozzle exit being 30 mm high and 0.5 m wide. The measured contraction ratio was unity (i.e. $d_o = 30$ mm). Earlier experiments showed that the flow was two-dimensional and fully developed at the first drop.

Water to the 3.2 m long channel was supplied by an adjustable sluice gate located 0.62 m upstream of the drop. The approach flow conditions were measured at vena contracta, and the flow was partially developed at the step brink: i.e., $\delta/d_o = 0.2 - 0.35$ where δ is the boundary layer thickness.

3 Flow regimes, cavity subpressure and nappe ventilation

3.1 Presentation

For all stepped chute experiments, the waters progressed as a succession of free-falling nappes with supercritical flow in between. Hydraulic jumps were not observed on any step. These flow characteristics appeared to match the classification of nappe flow without hydraulic jump as defined by Chanson (1995, 2001). The nappe flow on the cascade was observed to display three-dimensional flow patterns downstream of the first drop and on the subsequent steps. At nappe impact on the step, the change in flow direction resulted in the formation of sidewall standing-waves (a long narrow "bow-wave" forming on each sidewall downstream of nappe impact) and shockwaves in the downstream supercritical flow. These flow patterns are illustrated in Fig. 1 and discussed in the next paragraph.

For the largest flow rates ($0.9 < d_c/h < 1.0$), however, it was difficult to classify the flow regime as "nappe flow" in the classical sense. The flow clearly progressed as a series of discrete drops, but the absence of air cavity beneath the falling nappe implied a jet flow overflowing a recirculating pool of water somehow similar to "skimming flow". The low gradient (ratio h/l) of the cascade seemed to inhibit the formation of a classical "skimming flow regime", while downstream of nappe impact, the flow displayed properties similar to those observed for nappe flow. For these largest discharges ($0.8 \leq d_c/h < 1$), the flow regime was thought to be a transition flow regime (e.g. Chanson and Toombes, 2004).

3.2 Cavity subpressures and nappe ventilation

In experiments Series 1, down the 25 m long cascade, all steps were not ventilated. The air cavity subpressure was measured at the first drop. Typical results are shown in Fig. 2, where $\Delta P = P_{atm} - P_{cavity}$, and d_o and Fr_o are the inflow depth and Froude number, respectively. For low flow rates ($Fr_o \leq 4.8$ corresponding to $d_c/h \leq 0.6$), the cavity subpressure was basically independent of flow rate, while it decreased with increasing discharge for larger flow rates ($Fr_o \geq 5$) (Fig. 2).

Although it could be expected that the suction pressure increased with flow velocity for two-dimensional jets, it is proposed that nappe ventilation occurred next to the sidewall at high flow rates as a result of lateral nappe contraction. Since the velocity increases in the free-falling nappe, the flow cross-sectional area must decrease by continuity and it was observed that the nappe tended to contract away from the sidewalls. In addition, any small roughness of the chute sidewall (e.g. a joint) could cause a jet deflection, generating a gap between nappe and wall which would contribute to some nappe ventilation. The

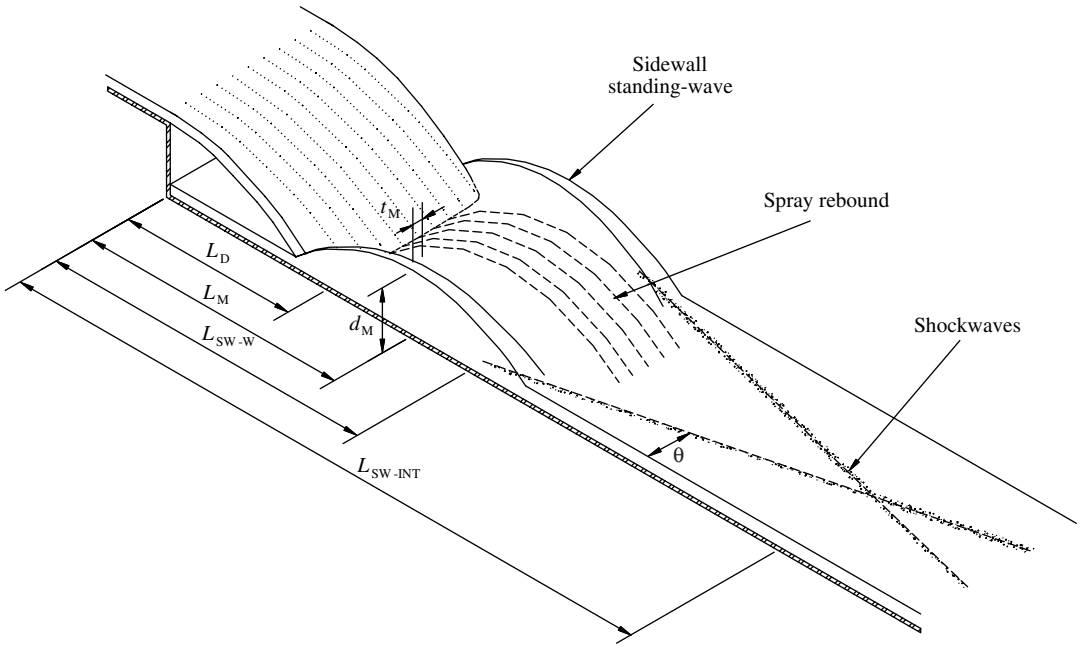

(a)

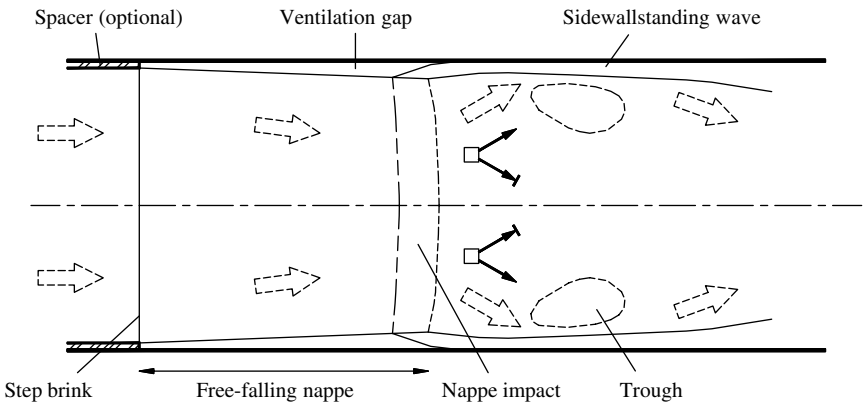

(b)

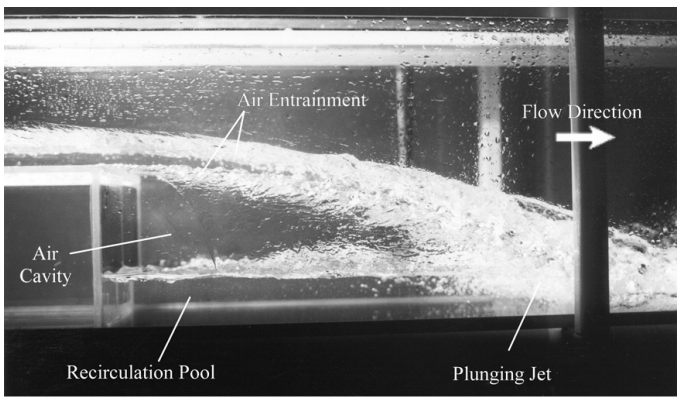

(c)

Figure 1 Nappe flow without hydraulic jump. (a) Definition sketch. (b) Sketch of free-jet, nappe contraction and flow expansion downstream of impact. (c) Free-falling jet: $d_c/h = 0.61$, inflow depth: 0.03 m, $h = 0.143$ m, $W = 0.25$ m high-shutter speed photograph (1/125zth s).

existence of air gap next to sidewall was evidenced by high air concentrations measured next to the sidewall. Further examination of air-concentration profiles through the free-falling nappe showed that, at the upstream end, there existed a clear-water, while downstream the air concentration in the central core was not zero. The finding suggested some air flux across the full thickness of the nappe. It is conceivable that the highly turbulent nature of the flow led to some transfer of air through the jet

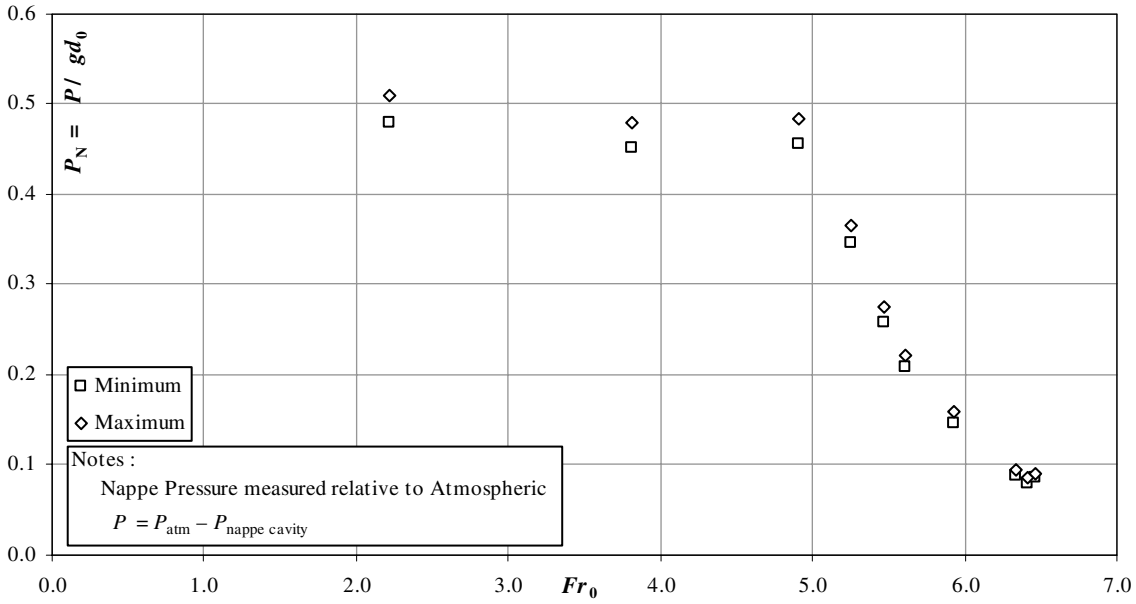

Figure 2 Dimensionless air cavity sub-pressure at the first drop (Experiments Series 1).

Table 2 Dimensionless subpressures of unventilated cavities: present study and spillway aeration device studies

Ref. (1)	Geometry (2)	Froude number (3)	$\frac{\Delta P}{\rho^* g^* d_o}$ (4)	$\frac{d_o}{h}$ (5)	Remarks (6)
CHANSON (1988)	$\phi = 5.7°$	13.30	0.4	0.95	Spillway aeration device.
$\theta = 51°$	$t_r = 0.03$ m	4.50	0.2	2.17	$W = 0.25$ m
	$h = 0.03$ m	5.63	0.25	2.17	
	$\phi = 0°$	9.36	0.3	0.95	
	$h = 0.03$ m	5.60	0.4	2.17	
TAN (1984)	$\phi = 4°$	6.4	0.2	1.67	Spillway aeration device.
$\theta = 51°$	$t_r = 0.026$ m				$W = 0.25$ m
	$h = 0.03$ m				
	$\phi = 0°$	5.0	0.4 to 0.5	1.67	
	$h = 0.03$ m				
Present study	$h = 0.143$ m	2 to 5	0.4 to 0.5	0.2	Stepped cascade.
$\theta = 3.4°$					$W = 0.25$ m

Notes: t_r: ramp height; ϕ: ramp angle with spillway invert.

from the upper to lower nappes. An analysis of air-concentration results suggested that little jet core aeration occurred for inflow Froude numbers less than 5. For $Fr_o > 5$, the length of clear-water core was comparatively smaller and the contraction of the nappe became significant. Both effects allowed progressively some air flux through and around the nappe.

At low flow rates, the dimensionless subpressure of unventilated cavity was of the same order of magnitude as that observed in experiments for non-ventilated nappes on spillway aeration devices for which nappe cavity pressures of $0.3 \leq \Delta P/\rho^* g^* d \leq 0.5$ were observed for ramp angles of $\phi = 0°$ (Table 2).

For all other experiments, nappe ventilation by sidewall splitters was provided in the 3.2 m long flume (experiments Series 3) and at the first drop in the 25 m long channel for experiments Series 2. The other steps were not ventilated.

4 Basic flow patterns

The flow on the low gradient stepped chute displayed complicated three-dimensional patterns. The flow properties changed rapidly on the upstream steps, until reaching some form of "quasi-equilibrium" on the lowest steps where the flow patterns and properties on each step appeared about identical to those on the preceding steps. Downstream of jet impact, the spray was highly fragmented with a large amount of spray concentrated towards the centreline of the channel. Standing-waves similar

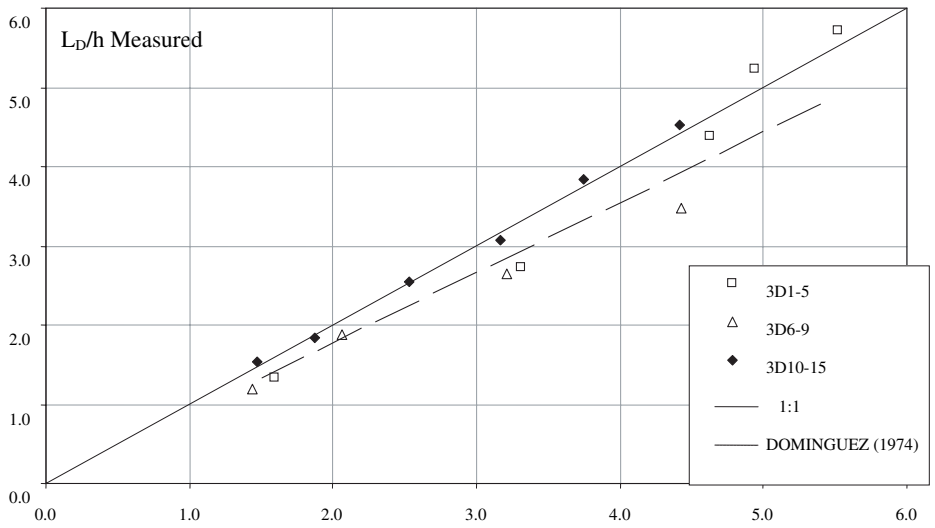

(a)

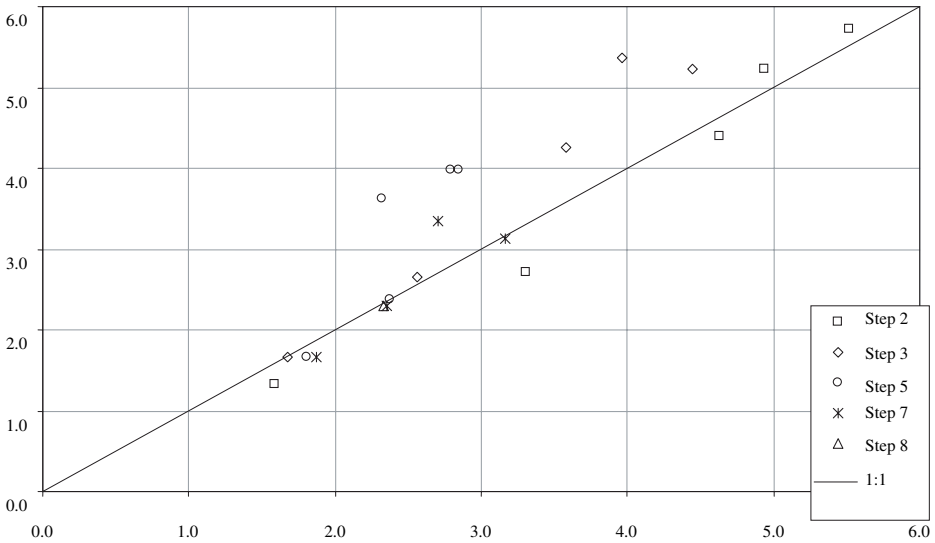

(b)

Figure 3 Dimensionless comparison between measurements (vertical axis) and calculated jet length (Eq. 1) (horizontal axis). (a) First drop (legend: 3D1-5 = experiments Series 1; 3D6-9 = experiments Series 2; 3D10-15 = experiments Series 3). (b) Subsequent drops (Experiments Series 1).

to bow-waves on a ship formed along the sidewalls downstream of nappe impact, and shockwaves were observed on each step, originating from the sidewall at, or close to, free-falling jet impact.

4.1 Jet length

The drop length of the free-falling nappe was observed to increase with the flow velocity. The trajectory of a free-falling, ventilated nappe may be derived from the energy equation (Marchi, 1993; Toombes, 2002) which yields the dimensionless drop length:

$$\frac{L_D}{h} = \frac{d_o}{2^*h} * \left(\sqrt{1 + (Fr_o^{-1} + 2^*Fr_o)^2 * \left(2^* \frac{h}{d_o} + \frac{d_b}{d_o} \right)} - 1 \right) \quad (1)$$

where d_o and Fr_o are the depth and Froude number upstream of the drop, d_b is the flow depth at the brink of the step and h is the height of the step. A comparison of measured drop length with theoretical drop length (Eq. 1) is shown in Fig. 3a for the first drop and Fig. 3b for the subsequent drops.

The first drop data compared favourably with Eq. (1) and experimental data obtained by Dominguez (1974). Comparison of jet length observed on subsequent steps with predicted length (Eq. 1) again demonstrated reasonable agreement as shown in Fig. 3b, although the measured drop lengths on Steps 3 and 5 tended to be greater than those predicted. Possible explanations might include the improper assumptions of two-dimensional jet with atmospheric cavity pressure.

4.2 Pool height

At nappe impact, the jet experienced a sudden change in direction (Fig. 1). For the present experiments, the impact angle of the jet with the horizontal was typically between 25° and 30°,

Table 3 Measured recirculating pool heights

Ref. (1)	h (m) (2)	d_o (m) (3)	Fr_o (4)	d_p/h (5)	Comments (6)
Series 1	0.1433				$W = 0.5$ m. Measurement with single-tip conductivity probe
		0.0336	4.4	0.42	
		0.0367	5.3	0.17	
		0.0326	8.5	<0.05 (∗)	(∗) Could not be measured
Series 3	0.1433				$W = 0.25$ m. Sidewall measurements
		0.0306	5.0	0.31	
		0.029	6.3	0.31	
		0.0296	7.0	0.31	
		0.0243	7.4	0.24	

Note: d_p: recirculating pool height measured on vertical step face.

depending on the jet flow conditions. A pool of water, formed immediately upstream of nappe impact, acted to provide a horizontal pressure force and satisfied the momentum balance at the impact. The characteristics of the impact region, including pool and downstream depth, were investigated by a number of studies (e.g. Moore, 1943; White, 1943; Chanson, 1995), although the majority focused on subcritical inflow conditions.

Present observations were compared with theoretical pool depth predictions developed by White (1943) and Chanson (1995), and an extension of White's development to account for sidewall spacers (Toombes 2002, pp. 182–185). Recirculating pool heights were measured through the sidewalls in experiments Series 3, and with a single-tip conductivity probe in experiments Series 1 (Table 3). In experiments Series 3, predictions based on Chanson's (1995) assumptions showed good agreement with the measured results for all flow rates, as well as in experiments Series 1 at lower velocities ($V_o < 3$ m/s). White's calculations gave a reasonable agreement, although they tended to underestimate the observed values.

There is no single obvious reason for the increasing disparity between theoretical results and measurements at higher flow rates in experiments Series 1. However, it must be noted that neither White (1943) nor Chanson (1995) accounted for air entrainment within the free-falling jet at, or downstream of, nappe impact, while the effects of an abrupt channel expansion on the velocity downstream of the impact were ignored.

4.3 Sidewall standing-waves and shock-waves

Sidewall standing-waves were observed downstream of the nappe impact. The standing-waves were comparable to similar phenomenon observed on the opposite wall of mitre bends and channel junctions (Schwalt and Hager, 1993), at abrupt channel expansions (Hager and Mazumder, 1992), and the bow-wave on ships (Waniewski, 1999). The standing-waves appeared to be generated by the impact of the lower nappe of the free-falling jet into the recirculating pool of water beneath the nappe (Chanson and Toombes, 1998). The height of sidewall standing-waves was appreciably higher than both inflow and downstream depths.

Air-concentration contours through the sidewall standing-wave on the single-step model are shown in Fig. 4, at several cross-sections downstream of nappe impact. In Fig. 4, all dimensions are scaled by the half-channel width ($W/2$) with x the longitudinal distance measured from the vertical step face, y the transverse distance measured from the centreline, z the vertical distance measured from the downstream step invert. Figure 4a occurred just downstream of nappe impact. The sidewall standing-wave was already partially developed. It must be noted that the presence of the pool of water beneath the free-falling nappe somewhat complicated the nappe impact on the step invert. Between $x = 0.7$ m and $x = 0.8$ m, the standing-wave height and the volume of spray ($C > 80\%$) increased significantly, peaking at around $x = 1.0$ m (Fig. 4c). Importantly the sidewall standing-wave was relatively narrow at all times and highly aerated, with $C > 25\%$ for most of its height. Note that, in Fig. 4b and c, the wave is slightly wider at top and bottom than in the middle, giving it some of the appearances of breaking-wave and bow-wave. In Fig. 4b and c, the formation of a "trough" region (i.e. low flow depth) is observed between $0.4 < Y < 0.8$ where $Y = 2 * y/W$. This trough can be clearly identified between $6.5 < X < 8.5$ in Fig. 5a where $X = x/d_o$.

Figure 5 presents dimensionless contours of air–water flow properties downstream of nappe impact. That is, contour maps of dimensionless clear-water flow depth d/d_o, depth-averaged void fraction C_{mean} and water flux $q_w/(V_o * d_o)$ where:

$$d = \int_{z=0}^{z_{90}} (1 - C) * dz \tag{2}$$

$$C_{mean} = \int_{z=0}^{z_{90}} C * dz \tag{3}$$

$$q_w = \int_{z=0}^{z_{90}} (1 - C) * V * dz \tag{4}$$

z_{90} is the air–water depth where $C = 90\%$, and C and V are the measured local void fraction and air–water velocity, respectively. Since the flow was three-dimensional, d, C_{mean} and q_w were functions of x and y. In Fig. 5, the dimensions are scaled in both directions with respect to half the channel width ($W/2$). (Note that although the dimensional scaling is identical in each

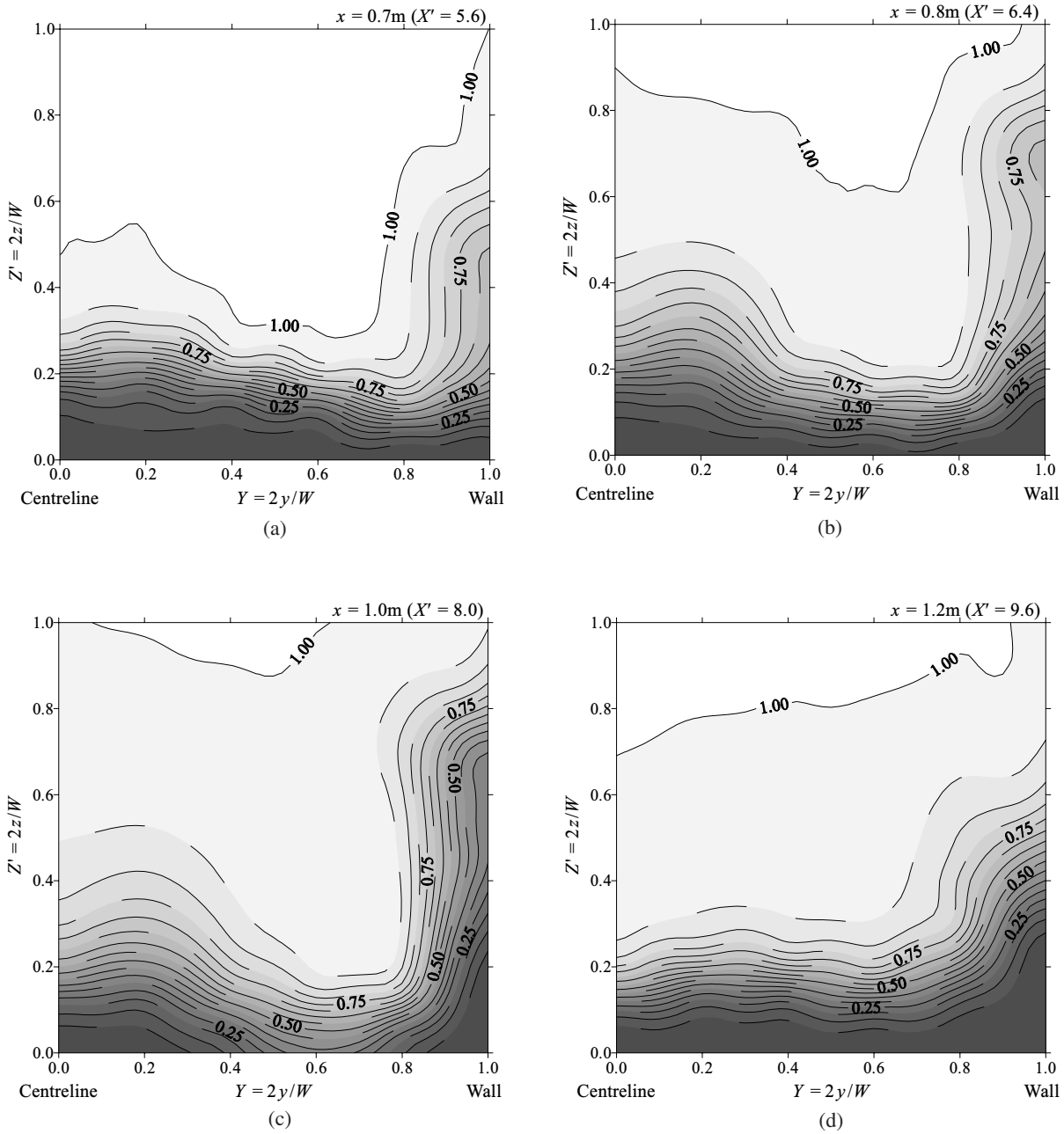

Figure 4 Dimensionless contour profiles of air concentrations through the flow downstream of nappe impact experiment series 3, $d_c/h = 0.64$, inflow depth : 0.0243 m, $h = 0.143$ m, $W = 0.25$ m. Legend: 3D1-5 = experiment series 1; 3D6-9 = experiment series 2; 3D10-15 = experiment series 3 (a) $x = 0.7$ m (b) $x = 0.8$ m (c) $x = 1.0$ m (d) $x = 1.2$ m.

direction, the presentation of the graph is distorted to exaggerate the y-direction). In Fig. 5, the sidewall standing-wave can be clearly identified as a region of large clear-water flow depth, generally bounded by $6 < X < 10$ and $0.9 < Y < 1.0$. Shockwaves propagated across the channel and the approximate position of the (upstream side of the) shockwave is marked with a dashed line in Fig. 5. Note that the downstream end of the sidewall standing-wave merged into the shockwave, suggesting that the two features were related. Downstream of the shockwave, the clear-water flow depth was greater than upstream of the shockwave.

The depth-averaged air concentration data (Fig. 5b) showed three main patches of high air concentration: within the spray region downstream of impact ($7 < X < 8.5$, $0 < Y < 0.7$), at the start of the sidewall standing-wave ($5 < X < 7.5$, $0.9 < Y < 1.0$) and at the tail of the sidewall standing-wave ($9 < X < 10$, $0.6 < Y < 0.85$). The latter area may be related to the collapse of the sidewall standing-wave, and a vertical section through this region is shown in Fig. 4d. It should be noted that high air concentrations were measured upstream of the shock waves. Significant de-aeration occurred within the shockwaves, and some de-aeration continued further downstream. The dimensionless local water flux $q_w/(V_o * d_o)$ is shown in Fig. 5c. Between $5 < X < 10$, there was a distinct concentration of flow at the sidewall and on the centreline, leaving a trough from $0.4 < Y < 0.85$. For $10 < X < 15$, there was a net flow from the sidewall

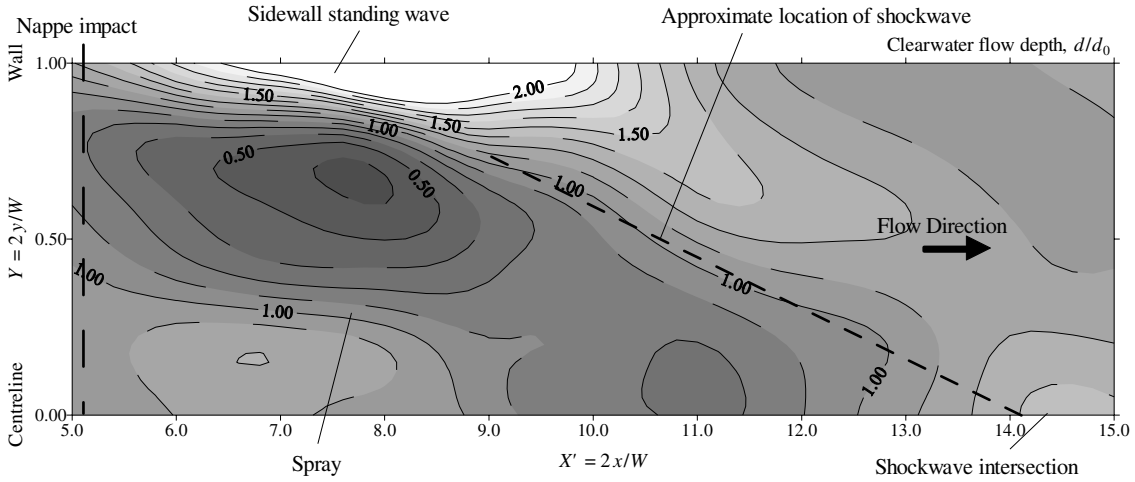

(a)

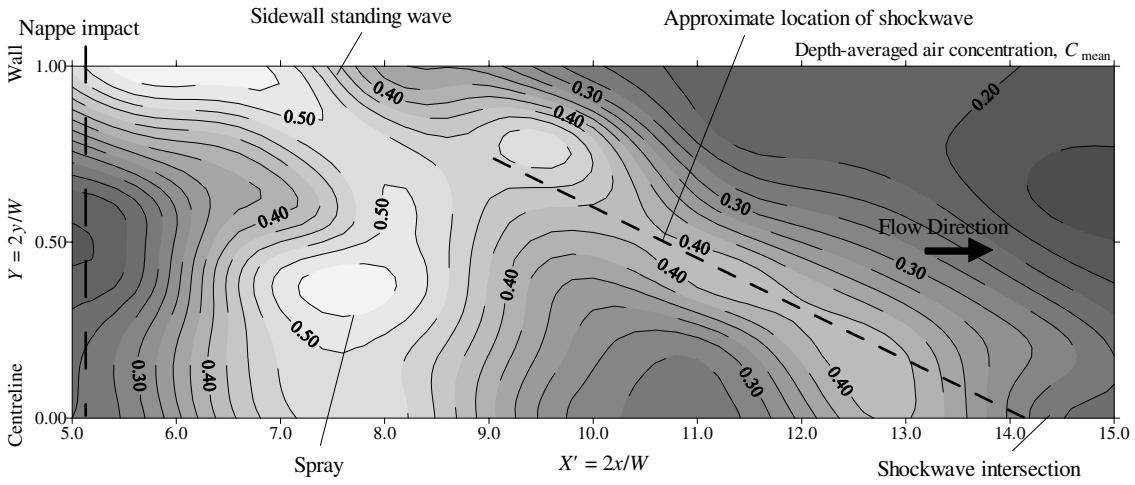

(b)

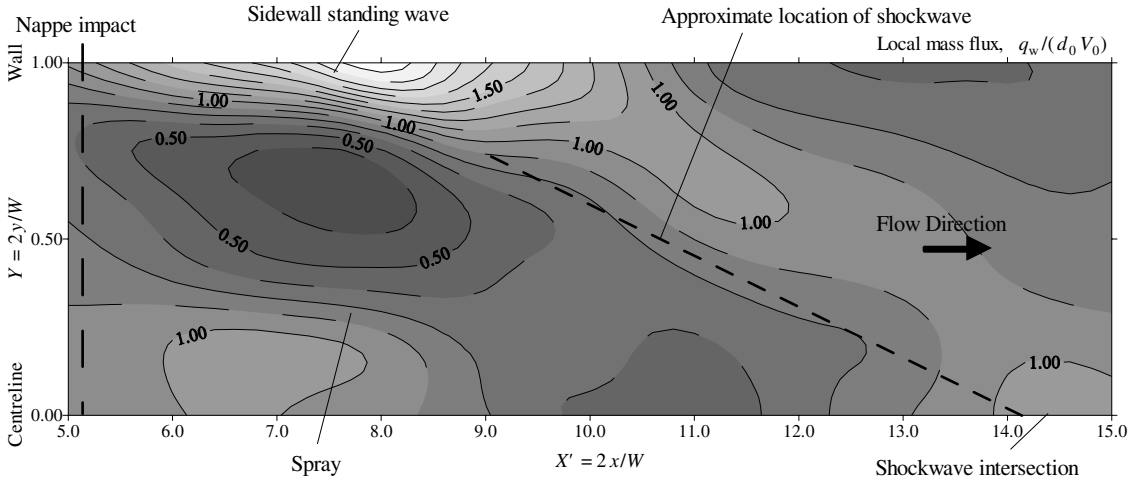

(c)

Figure 5 Dimensionless contour lines of air–water flow properties downstream of nappe impact experiment series 3, $d_c/h = 0.64$, inflow depth : 0.0243 m, $h = 0.143$ m, $W = 0.25$ m. (a) Dimensionless equivalent clear water flow depth d/d_o. (b) Depth-averaged air concentration C_{mean}. (c) Dimensionless water flux $q_w/(d_o * V_o)$.

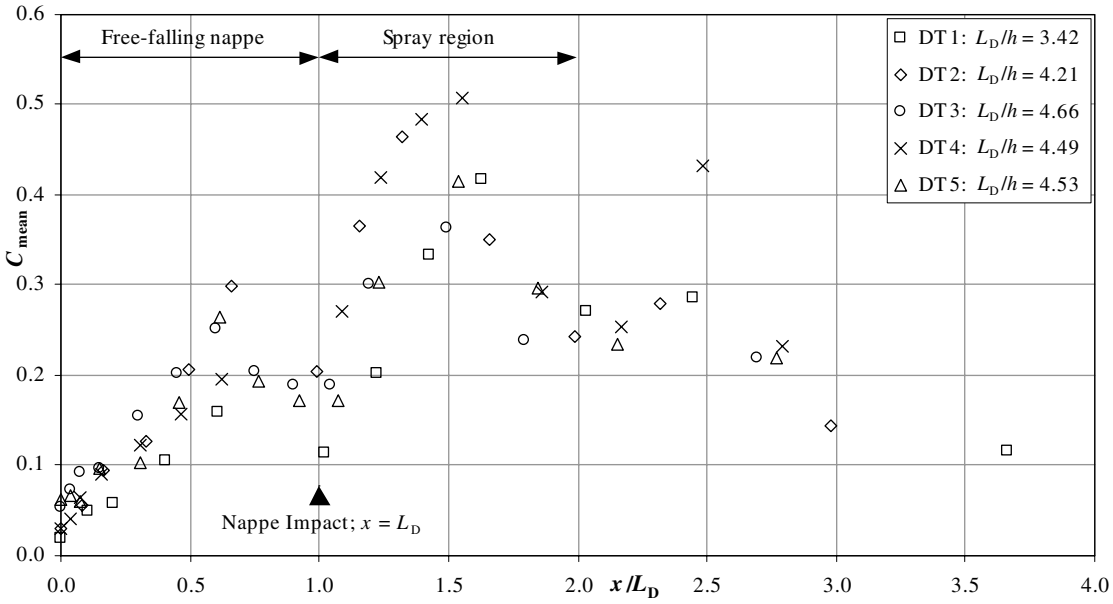

Figure 6 Longitudinal variations of depth-averaged air concentration on the channel centreline downstream of the step brink. Experiment series 3: $d_c/h = 0.62$ (DT1), 0.69 (DT2), 0.75 (DT3), 0.64 (DT4), 0.89 (DT5).

standing-waves towards the channel centreline, showing that the shockwaves induced some flow concentration.

4.4 Discussion

Sidewall standing-waves are commonly observed at channel bends or where the flow is forced to change direction. It is hypothesized that the formation of both sidewall standing wave and free-surface trough was the result of contraction of the free-falling jet and subsequent expansion upon impact. At jet impact, the nappe may to expand laterally to form a fan shape if it is not constrained laterally (Fig. 1b). Consider an element of fluid downstream of nappe impact, it is somewhat free to expand somewhat towards the sidewalls because of some gap resulting from free-jet contraction. Upon encountering the sidewall, the flow is forced up, forming a standing-wave. There is a net flux of flow away from the centreline into the sidewall standing-waves, leaving the trough. The water returns to fill this trough as the sidewall standing-wave collapses further downstream. Evidence of this flow flux pattern is found in Fig. 5c.

Downstream of nappe impact, a percentage of the impacting waters tended to separate upwards from the main flow, resulting in the formation of a large volume of spray and entrainment of air next to the channel centreline. The spray ejected immediately downstream of nappe impact, it followed a somewhat ballistic trajectory and rejoined the main flow further downstream (Fig. 1a). The depth-averaged air concentration consequently reached a maximum next to the peak of the spray trajectory, then decreased towards the end of the step. The spray region was typically girt by standing-waves on each sidewall. The depth-averaged air concentration within the spray region is typically $0.25 < C_{mean} < 0.5$ on the channel centreline (Fig. 6). This is illustrated in Fig. 6 showing the longitudinal variations of centreline depth-averaged air content C_{mean}. The maximum depth-averaged air concentration, typically $0.4 < C_{mean} < 0.5$, was over twice the air concentration observed at the downstream end of the step.

5 Summary and conclusion

New experiments were conducted in nappe flows without hydraulic jump in two large-size facilities with low gradients. The flow on the stepped cascade displayed complex, three-dimensional patterns. The flow properties changed rapidly on the upstream steps, until reaching a form of "quasi-equilibrium" on the lower steps where the flow patterns and properties on each step were virtually identical to those on the preceding steps. The drop length of the free-jet was reasonably predicted from Eq. (1), which is based upon the energy equation. Downstream of nappe impact, the spray became highly fragmented with a large amount of spray concentrated towards the centreline of the channel. Standing waves similar to bow waves on a ship formed on the sidewalls downstream of nappe impact. The flow on the cascade remained supercritical everywhere, and shockwaves were observed on each step, originating on the sidewall at, or close to, nappe impact.

Detailed air–water flow measurements were performed in the jet, at nappe impact and in the downstream flow region. Results showed a three-dimensional distribution of air–water flow properties. The depth-averaged air concentration increased rapidly over a short distance immediately downstream of nappe impact. Although some air was entrained by plunging jet action where the lower nappe impacted into the recirculating pool, a significant volume of spray was generated by the impact onto the step. The centreline mean air concentration typically peaked at $40\% < C_{mean} < 50\%$ at a distance of approximately 1.5 times the drop length downstream of the step brink. The depth-averaged air concentration decreased further downstream as the spray

progressively rejoined the main flow and entrained air-bubbles were expelled, while some flow de-aeration took place along the shock waves.

A key result is that the flow on each step was rapidly varied (RVF), highly three-dimensional and strongly aerated. It is believed that further studies under controlled flow conditions are required to gain a complete understanding of these complicated air-water flow patterns, while field observations must be obtained to validate any extrapolation of such laboratory observations.

Acknowledgments

The first writer acknowledges the financial support of the Australian Research Council and of the University of Queensland. The writers are grateful of the helpful comments from the reviewers.

Notation

C = Air concentration
C_{mean} = Depth-averaged air concentration
d = (1) flow depth (m) measured normal to the step invert
(2) equivalent clear-water flow depth (m)
d_b = Brink depth (m)
d_c = Critical flow depth (m)
d_o = Inflow depth (m)
Fr = Froude number defined as : $Fr = V/\sqrt{g * d}$
Fr_o = Inflow Froude number
g = Gravity acceleration (m/s^2)
h = Height of steps (m) (measured vertically)
L_D = Jet length (m)
l = Step length (m)
P = Pressure (Pa)
P_{atm} = Atmospheric pressure (Pa)
P_{cavity} = Air cavity pressure (Pa)
q_w = Depth-averaged water flux (m^2/s)
Re = Reynolds number defined in terms of hydraulic diameter
S_o = Bed slope
V = Velocity (m/s)
V_o = Inflow velocity (m/s)
W = Channel width (m)
X = Dimensionless longitudinal distance: $X = x/d_o$
X' = Dimensionless longitudinal distance: $X' = 2 * x/W$
x = Longitudinal distance (m) measured from the step vertical face
Y = Dimensionless transverse distance: $Y = 2 * y/W$
y = Transverse distance (m) measured from the channel centreline
Z = Dimensionless vertical distance: $Z = z/d_o$
Z' = Dimensionless longitudinal distance: $Z' = 2 * x/W$
z = Vertical distance (m) measured from the step invert
z_{90} = Vertical distance (m) measured from the step invert where $C = 0.90$

Greek symbols

ΔP = Air pressure subpressure (Pa)
δ = Boundary layer thickness (m)
θ = Channel slope

Subscript

o = Inflow conditions

References

1. CHAMANI, M.R. and RAJARATNAM, N. (1994). "Jet Flow on Stepped Spillways". *J. Hydraul. Engg. ASCE* 120(2), 254–259.
2. CHANSON, H. (1988). "A Study of Air Entrainment and Aeration Devices on a Spillway Model". Ph.D. Thesis, Ref. 88-8, Department of Civil Engineering, University of Canterbury, New Zealand.
3. CHANSON, H. (1994). "Hydraulics of Nappe Flow Regime above Stepped Chutes and Spillways". *Aust. Civil Engg. Trans. I.E.Aust.* CE36(1), 69–76.
4. CHANSON, H. (1995). *Hydraulic Design of Stepped Cascades, Channels, Weirs and Spillways*. Pergamon, Oxford, UK.
5. CHANSON, H. (2001). "The Hydraulics of Stepped Chutes and Spillways". Balkema, Lisse, The Netherlands, 418 pp.
6. CHANSON, H. and TOOMBES, L. (1998). "Supercritical Flow at an Abrupt Drop: Flow Patterns and Aeration". *Can. J. Civil Eng.* 25(5), 956–966.
7. CHANSON, H. and TOOMBES, L. (2004). "Hydraulics of Stepped Chutes: The Transition Flow". *J. Hydraul. Res. IAHR* 42(1), 43–54.
8. DOMINGUEZ, F.J. (1974). *Hidraulica* ("*Hydraulics*"), 4th edn. Editorial Universitataria, Santiago, Chile, (in Spanish).
9. HAGER, W.H. and MAZUMDER, S.K. (1992). "Supercritical Flow at Abrupt Expansions". *Proc. Instn. Civ. Engrs. Wat. Marit. Ener.* UK, Vol. 96, Sept., pp. 153–166.
10. HORNER, M.W. (1969). "An Analysis of Flow on Cascades of Steps". Ph.D. Thesis, University of Birmingham, UK, May, 357 pp.
11. MARCHI, E. (1993). "On the Free-Overfall". *J. Hydraul. Res. IAHR* 31(6), 777–790.
12. MOORE, W.L. (1943). "Energy Loss at the Base of a Free Overfall". *Trans. ASCE* 108, 1343–1360.
13. PINHEIRO, A.N. and FAEL, C.S. (2000). "Nappe Flow in Stepped Channels—Occurrence and Energy Dissipation". *International Workshop on Hydraulics of Stepped Spillways*, Balkema Publ., pp. 119–126.

14. SCHWALT, M. and HAGER, W.H. (1993). "Supercritical Flow Deflection". *Proc. 25th IAHR Congress*, Tokyo, Japan, Session A, Vol. I, pp. 345–352.
15. TAN, T.P. (1984). *Model Studies of Aerators on Spillways*. Research Report No. 84–6, University of Canterbury, Christchurch, New Zealand.
16. TOOMBES, L. (2002). "Experimental Study of Air–Water Flow Properties on Low-Gradient Stepped Cascades". *Ph.D. Thesis*, Department of Civil Engineering, The University of Queensland.
17. WANIEWSKI, T.A. (1999). "Air Entrainment by Bow Waves". Ph.D. Thesis, California Institute of Technology, Pasadena, California.
18. WHITE, M.P. (1943). "Energy Loss at the Base of a Free Overfall—Discussion". *Trans. ASCE* 108, 1361–1364.